Robotica: (2021) volume 39, pp. 524–534. © The Author(s), 2020. Published by Cambridge University Press.
doi:10.1017/S0263574720000545

Linear Quadratic Regulator Method in Vision-Based Laser Beam Tracking for a Mobile Target Robot

Yun Ling†*, Jian Wu†, Weiping Zhou‡, Yubiao Wang† and Changcheng Wu¶

†*Nanjing Research Institute of Simulation Technology, Department of Research Center, Nanjing, Jiangsu*
‡*Nanjing Research Institute of Simulation Technology, Department of Combat Training, Nanjing, Jiangsu*
¶*Nanjing University of Aeronautics and Astronautics, College of Automation Engineering, Nanjing, Jiangsu*

(Accepted June 7, 2020. First published online: July 3, 2020)

SUMMARY
This paper proposes a novel laser beam tracking mechanism for a mobile target robot that is used in shooting ranges. Compared with other traditional tracking mechanisms and modules, the proposed laser beam tracking mechanism is more flexible and low cost in use. The mechanical design and the working principle of the tracking module are illustrated, and the complete control system of the mobile target robot is introduced in detail. The tracking control includes two main steps: localizing the mobile target robot with regards to the position of the laser beam and tracking the laser beam by the linear quadratic regulator (LQR). First of all, the state function of the control system is built for this tracking system; second, the control law is deduced according to the discretized state function; lastly, the stability of the control method is proved by the Lyapunov theory. The experimental results demonstrate that the Hue, Saturation, Value feature-extracting method is robust and is qualified to be used for localization in the laser beam tracking control. It is verified through experiments that the LQR method is of better performance than the conventional Proportional Derivative control in the aspect of converge time, lateral error control, and distance error control.

KEYWORDS: Laser beam; Path tracking; Indoor localization; LQR; Target robot

1. Introduction

Nowadays, owing to the urgent requirements of the military modernization and the worsened situation of anti-terrorism, the intelligentized firing practice systems in shooting ranges play an increasingly important role.[1] In order to effectively improve the combat capability of the police officers and soldiers, the advanced training subjects are developed, and the mobile target robots are utilized to achieve higher fidelity.

1.1. Development of indoor localization

In the modern training subjects, it is of high frequency to construct a scene in which an enemy or a terrorist is rushing towards the trainees from somewhere. The traditional fixed targets are not qualified to simulate this situation. Although the image targets demonstrate it perfectly, it is lack of oppressing sensation and scene fidelity. To satisfy the requirement, an intelligent robot with a movable target is

* Corresponding author. E-mail: lingrobot@seu.edu.cn

https://doi.org/10.1017/S0263574720000545 Published online by Cambridge University Press

designed. For those mobile target robots which are used to achieve more complicated movements, local positioning systems, like the Ultra-Wide Bandwidth positioning system,[2] the Radio Frequency Identification system,[3] the Adaptive Monte Carlo Localization using range finder or Light Detection and Ranging,[4] and the vision positioning systems,[5] are adopted to realize more advanced functions, for example, the tactical behaviors and the cooperative combats. However, for those mobile target robots which are used in the rushing-out simulation, the complicated positioning systems, which require higher calculation power and cost, are not suitable anymore.

Localization during path tracking is one of the key technologies in mobile robot applications. For the simple robot systems used in shooting ranges, previously drawing lines on the ground[6] or installing positioning devices[7] on the ground is the most commonly used approach. These tracking methods are used to make it possible for the mobile target robot to rush from some corner to the trainees. However, the constraints and disadvantages of these methods are obvious: the guide lines are immovable, and have to be cleared and drawn again when the rushing paths have been changed. Moreover, the line on the ground gives the trainees a psychological hit that the mobile target robot will rush out along it. The effect of these factors on training quality is ignorable. As for magnetic guiding or similar methods, fixing these components on the ground is a heavy work, which has the same disadvantage of immovable.

In order to solve these problems, the paper proposes a novel method, which uses laser beam as the guide line, and uses cameras to capture the relative position between the laser beam and the mobile target robot, that is, localization, for the tracking control. The laser transmitter, which is used to transmit the laser beam, can be placed anywhere, and hence it is very easy to change the working place for the mobile target robot.

1.2. Path tracking methods for mobile robots

Path tracking is one of the key technologies in mobile robot navigation. An angular velocity controller, which takes the linear velocity control into the control law design, was proposed and applied in a Stanley robot.[8] The Stanley controller is feasible for the control of the Ackermann-type robots. The conventional Proportional-Integral-Derivative (PID) control and the improved control algorithms based on the PID, for example, the fuzzy PID, were proposed for the path tracking control of the mobile robots.[9,10] The active disturbance rejection control was developed to estimate and compensate for the effect of slip to improve the path tracking performance of the autonomous ground vehicles and robots.[11] The experiments, which compare the model predictive control with the conventional Proportional Derivative (PD) control, were carried out for the path tracking of the mobile robot.[12] The performance of the model predictive control is better than that of the PID control in simulation. Nevertheless, the feasibility in practical application still needs study. The sliding model control algorithm was adopted and implemented in the tracking control of the mobile robots and other types of ground vehicles.[13] However, how to construct an accurate model and handle with the oscillation around the equilibrium point are still worth further studying. The backstepping method is also one of the methods for the path tracking control of the mobile robots,[14] and the most difficult problem is the design of a suitable control law. The linear quadratic regulator (LQR) was introduced in the tracking control,[15] and it can handle with the nonlinear system via the Taylor expansion.

In addition to conventional control methods, there are some other kinds of control approaches, such as the dynamic window approach (DWA),[16] which finds the optimal control values in every single control step by scoring a series of the predicted trajectories of the robot. Concerns are raised that the control methods based on machine learning are introduced in the path tracking control. The neural network control was proposed to solve the tracking problem of mobile robots,[17] but there is still a long way to go to achieve the real-time computation and the robustness in the practical use. The reinforcement learning control could be a competitive way since it can be used in the motion control without system model.[18] Similar to the problems in the neural network control, the real-time performance and the robustness in control have to be guaranteed before application.

Among those control methods, the PD control is chosen for laser beam tracking. The PD control, which does not need a model and can be applied easily, is the most widely used control method in engineering. In addition, the LQR is adopted in laser beam tracking as well for the reason that the error of localization could be very small in the tracking process while the robot is not off the laser

https://doi.org/10.1017/S0263574720000545 Published online by Cambridge University Press

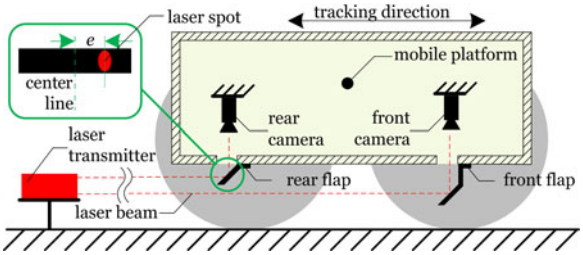


Fig. 1. Side view of the laser beam tracking module.

beam, and hence the Taylor expansion for linearization could be more accurate, which is probably the key point for its application for nonlinear control systems.

2. Tracking mechanism and control system design

2.1. Mechanism design of the laser beam tracking module

The laser beam tracking module is mainly composed of three components, namely the laser transmitter, the cut-beam flaps, and the low-cost cameras, as shown in Fig. 1. The laser transmitter transmits a planar (which is fan-shaped from the side view) laser beam, which is respectively cut off by two cut-beam flaps, namely the front flap and the rear flap that are fixed to the bottom of the target robot.

The laser beam projects one laser spot for each cut-beam flap. It is known that the laser beam is a directional light; therefore, the width of the laser spot projected on the cut-beam flap changes little when the mobile target robot moves back and forth.

Two rectangular orifices are located just above the flaps, so that the cameras installed above the flaps can observe the flaps. The poses of both cut-beam flaps are critical in achieving position perception of the laser spots. As seen in Fig. 1, the angle between the surface of the flap and that of the bottom plane of the mobile target robot is 45°, and their contact line is perpendicular to the tracking direction. Due to the 45°-fixed flaps, the cameras can well detect the laser spots on the flaps. Once the laser transmitter is fixed, the laser spots, which are captured by both cameras, shift accordingly on the flaps when the mobile target robot moves with a lateral deviation. Note that the cut-beam flap must not be specular such that the camera above can capture the spot on it, no matter which direction the laser transmits from.

2.2. Control structure of the robot

The mobile target robot is an integrated system and has the functions such as the path tracking control, target scoring, target flipping control, obstacles detection, parameters loading from the client, and the remote control, as shown in Fig. 2. The entire control system of the mobile target robot is composed of three main controllers: a target controller, a main controller, and a wheel velocity controller.

The target controller is designed to achieve target scoring, turn over the target, and send the suggested velocity commands to the main controller for motion control. For example, the target controller lays down the target and sends a stop suggestion to the main controller instantly when the critical part of the target (like the head or the heart) has been hit.

The main controller consists of a distance detector, an image processor unit, a distance error observer, a tracking control module, and a velocity control multiplexer. The distance error observer is constructed to compute the distance between the referenced position and the actual position of the robot. Then, the tracking control module, using the laser spot biases provided by the image processor, computes the linear and angular velocities, and generates the target velocities for the left-side and right-side wheels. Lastly, the velocity multiplexer receives the target velocity commands both from the tracking control module and the remote control, and judges which one should be adopted and sent to the velocity closed-loop controller.

The velocity closed-loop controller receives the final target velocities of the left-side and right-side wheels. The actual velocities, which are sampled from the encoders equipped on motors, are used to perform a higher-frequency velocity PD control.

https://doi.org/10.1017/S0263574720000545 Published online by Cambridge University Press

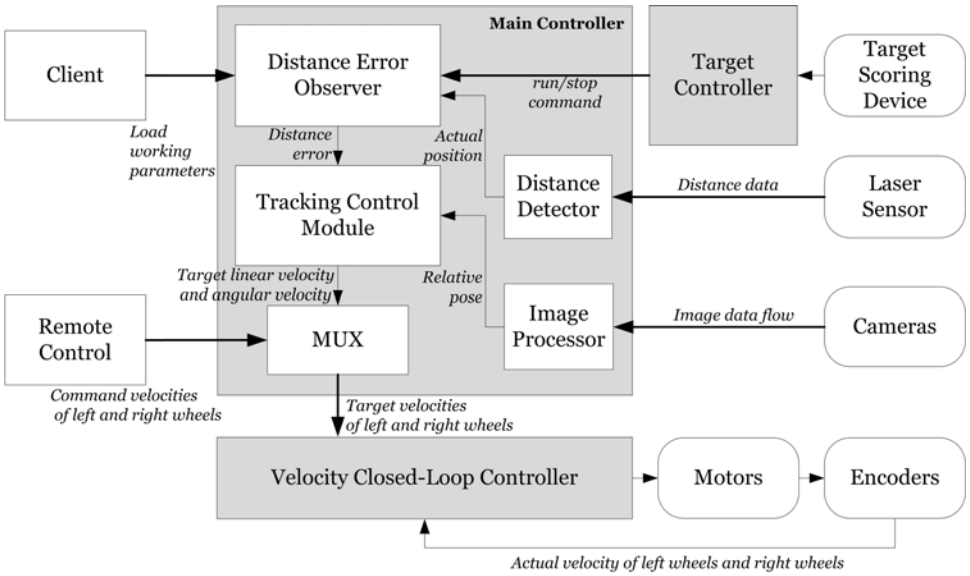


Fig. 2. Block diagram of the control system.

3. Localization via image processing

3.1. Region of interest selection

The image sizes captured by the cameras are both 640 × 480 pixels. According to the relationship between the field of view of the camera and the size and position of the cut-beam flaps, the region of interest (ROI) is a rectangular area at the center of the image. Thus, the image must be properly cropped by the following equation, so as to exclude the useless pixels:

$$U = \frac{l}{h \cdot \tan \frac{\varphi}{2}} \cdot X \tag{1}$$

where U is the length of the ROI image in x-direction (in which the laser spot shifts) after cropping, l denotes the length of both cut-beam flaps, h denotes the height of the lens of the cameras, φ denotes the camera's field of view in the x-direction, and X is the length of the original image in x-direction. After the calculation similar to Eq. (1) in y-direction, the size of the ROI is set to $[X/2 - U, X/2 + U; Y/2 - V, Y/2 + V]$ when the origin of the image matrix is at top left.

3.2. Hue, Saturation, Value (HSV) feature extraction and spot recognition

The cut-beam flaps are designed to be installed beneath the mobile target robot, so as to reduce the influence from ambient light. The conventional positioning method is well qualified to detect the position of the laser spot when the mobile target robot is working in the indoor shooting ranges. However, a better feature-extraction method should be developed to distinguish the laser spot from ambient light when it is ignorable or when the target robot is working outdoors.

It is known that the HSV color features are more stable against the changes of light intensity. Therefore, the image is first converted to the HSV format by the equation given as follows.[19] The hue is calculated by:

$$f_h = \begin{cases} 0, & \Delta = 0 \\ 60 \times \left(\frac{G' - B'}{\Delta} \bmod 6 \right), & C_{\max} = R' \\ 60 \times \left(\frac{B' - R'}{\Delta} + 2 \right), & C_{\max} = G' \\ 60 \times \left(\frac{R' - G'}{\Delta} + 4 \right), & C_{\max} = B' \end{cases} \tag{2}$$

https://doi.org/10.1017/S0263574720000545 Published online by Cambridge University Press

The saturation is calculated by:

$$f_s = \begin{cases} 0, & C_{\max} = 0 \\ \frac{\Delta}{C_{\max}}, & C_{\max} \neq 0 \end{cases} \tag{3}$$

And the value is given as:

$$f_v = C_{\max} \tag{4}$$

where R', G', and B' indicate $f_r(u, v)$, $f_g(u, v)$, and $f_b(u, v)$, respectively. $C_{\max} = \max(R', G', B')$ and $C_{\min} = \min(R', G', B')$. $\Delta = C_{\max} - C_{\min}$.

The binary image is computed by the following equation provided that the HSV ranges of the laser spots have been set.

$$f(u, v) = \begin{cases} 255\,, f_h \in [h_0 - \Delta h, h_0 + \Delta h] \bigcap f_s \in [s_0 - \Delta s,\ s_0 + \Delta s] \\ 0\,, \text{others} \end{cases} \tag{5}$$

where h_0 and s_0 are the thresholds of hue and saturation. Δh and Δs indicate the tolerances of the ranges.

After that, the binary image is processed by using morphological operations to erase small background noise and smooth the spot boundary without changing its size. The operation is described as:

$$A \circ B = (A \Theta B) \oplus B \tag{6}$$

where A is the binary image and B is a $m \times n$ kernel. The symbol Θ means the erode operation and the symbol $\oplus$ means the dilate operation.

The position of the laser spot in each row has a maximum width.[20] Based on this fact, the position of the spot in each row is calculated by the equation expressed as:

$$p_u = p^s + \frac{\max(\Delta l_v)}{2},\ where\ \Delta l_v = \{p_v^e - p_v^s\},\ v \in \Phi' \tag{7}$$

where p_v^s is the start position of the white pixel (with the value of 255) and p_v^e is the end position of the white pixel. Φ' indicates the candidate rows whose Δl_v is in a reasonable range. p^s is the start position of the white band of the maximum Δl_v in each row.

3.3. Tracking error observation

The relative position relationship between the mobile target robot and the laser beam is computed, provided that the laser spots on the front and rear cut-beam flaps have been located. The bias of each laser spot from the center line of the cut-beam flap e can be calculated by:

$$e = f(u) \cdot (p_u - \frac{U}{2}) \tag{8}$$

where $f(u)$ is a nonlinear scalar function whose variable is the bias of the laser spot in the image, and the value of the function is a scalar which indicates the ratio of the actual distance of the laser spot that deviates from the center of the cut-beam flap and the pixel distance of the bias in the image. The actual lateral bias of the laser spot on the front beam-cut board and that on the rear cut-beam flap are represented by e_f and e_r, respectively.

The relationship between the deviation of the mobile target robot and the biases of the laser spots on two flaps is illustrated in Fig. 3. We define the bias as negative when the laser spot is on the left side (facing the transmitting direction of the laser beam) for both the flaps. For the mobile target robot, the lateral position error e_{dis} and the orientation error e_{ori} are given as follows:

$$e_{dis} = \frac{e_f + e_r}{2} \tag{9}$$

$$e_{ori} = \arctan\left(\frac{e_f - e_r}{L}\right) \tag{10}$$

where L is the distance between two cut-beam flaps.

https://doi.org/10.1017/S0263574720000545 Published online by Cambridge University Press

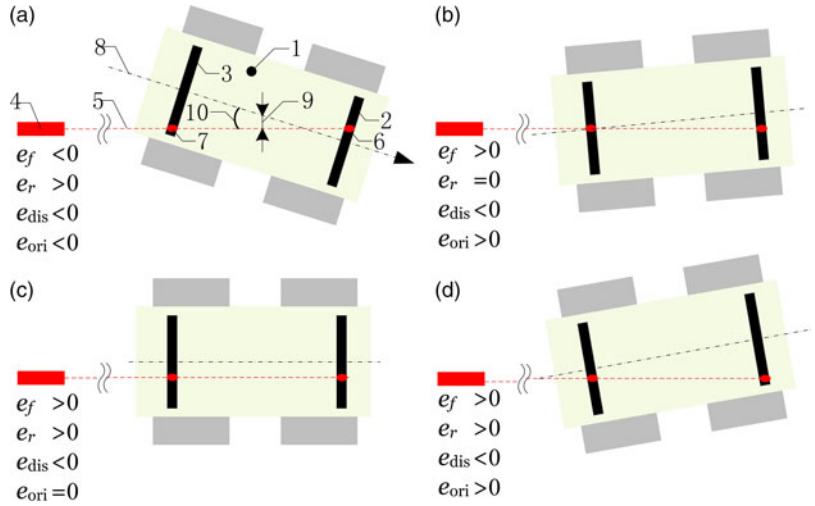


Fig. 3. Relative position relationship between the deviation of the mobile target robot and the biases of the laser spots on two flaps. 1 – mobile target robot; 2 – front cut-beam flap; 3 – rear cut-beam flap; 4 – laser transmitter; 5 – laser beam; 6 – front laser spot; 7 – rear laser spot; 8 – center line of the mobile target robot; 9 – lateral distance error; 10 – orientation error.

4. LQR-based laser beam tracking control

We define the pose of the robot as $\boldsymbol{X} = [x, y, \theta]^{\mathrm{T}}$. Then, the differential equation of the pose can be written as:

$$\dot{\boldsymbol{X}} = \begin{bmatrix} \dot{x} \\ \dot{y} \\ \dot{\theta} \end{bmatrix} = \begin{bmatrix} v\cos\theta \\ v\sin\theta \\ \omega \end{bmatrix} = f(\boldsymbol{X}, \boldsymbol{u}) \tag{11}$$

where v and ω are the linear and angular velocities of the robot. $\boldsymbol{u} = [v, \omega]^{\mathrm{T}}$.

Let $\boldsymbol{u}_r$ denote the referenced control output, in which v_r and ω_r are the referenced linear and angular velocities. Let $\boldsymbol{X}_r$ denote the referenced pose of the robot. Thus, the Taylor expansion of Eq. (11) can be deduced as following after neglecting the higher-order terms:

$$\dot{\boldsymbol{X}} = f(\boldsymbol{X}_r, \boldsymbol{u}_r) + \left.\frac{\partial f}{\partial \boldsymbol{X}}\right|_{\substack{X = X_r \\ u = u_r}} (\boldsymbol{X} - \boldsymbol{X}_r) + \left.\frac{\partial f}{\partial \boldsymbol{u}}\right|_{\substack{X = X_r \\ u = u_r}} (\boldsymbol{u} - \boldsymbol{u}_r) \tag{12}$$

The state function of the control system can be deduced from Eqs. (11) and (12) as:

$$\Delta\dot{\boldsymbol{X}}(t) = \boldsymbol{A}'(t)\Delta\boldsymbol{X}(t) + \boldsymbol{B}'(t)\Delta\boldsymbol{u}(t) \tag{13}$$

where $\Delta\boldsymbol{X}(t) = [x - x_r, y - y_r, \theta - \theta_r]^{\mathrm{T}}$ and $\Delta\boldsymbol{u}(t) = [v - v_r, \omega - \omega_r]^{\mathrm{T}}$.

The state equation of the control system is deduced as follows after discretization.

$$\begin{aligned} \Delta\boldsymbol{X}(k+1) &= [\boldsymbol{A}(k) \cdot dt + \boldsymbol{I}] \cdot \Delta\boldsymbol{X}(k) + (\boldsymbol{B}(k) \cdot dt) \cdot \Delta\boldsymbol{u}(k) \\ &= \boldsymbol{A}(k)\Delta\boldsymbol{X}(k) + \boldsymbol{B}(k)\Delta\boldsymbol{u}(k) \end{aligned} \tag{14}$$

where dt represents the control period.

Given the state equation, the optimal control can be obtained as follows:

$$\begin{aligned} \boldsymbol{u}* &= \boldsymbol{u}_r + \Delta\boldsymbol{u} = \boldsymbol{u}_r - \boldsymbol{K} \cdot \Delta\boldsymbol{X} \\ &= \boldsymbol{u}_r - \boldsymbol{R}^{-1}\boldsymbol{B}^{\mathrm{T}}(t)\boldsymbol{P}(t) \cdot \Delta\boldsymbol{X} \end{aligned} \tag{15}$$

where $P(t)$ is a positive definite matrix, which can be solved by the following Riccati equation for every control cycle.

$$\begin{aligned} &\dot{\boldsymbol{P}}(t) + \boldsymbol{P}(t)\boldsymbol{A}(t) + \boldsymbol{A}^{\mathrm{T}}(t)\boldsymbol{P}(t) \\ &\quad - \boldsymbol{P}(t)\boldsymbol{B}(t)\boldsymbol{R}^{-1}\boldsymbol{B}^{\mathrm{T}}(t)\boldsymbol{P}(t) + \boldsymbol{Q} = 0 \end{aligned} \tag{16}$$

https://doi.org/10.1017/S0263574720000545 Published online by Cambridge University Press



Fig. 4. Picture of the mobile target robot.

In order to prove that the control system is stable by applying Eq. (15), we define a Lyapunov function as follows:

$$V = \Delta \boldsymbol{X}^{\mathrm{T}}(t)\boldsymbol{P}(t)\Delta \boldsymbol{X}(t) \tag{17}$$

Substitute Eqs. (14)–(16) into Eq. (17), we obtain:

$$\dot{V} = -\Delta \boldsymbol{X}^{\mathrm{T}}(t)\{\boldsymbol{P}^{\mathrm{T}}(t)\boldsymbol{B}(t)(\boldsymbol{R}^{-1})^{\mathrm{T}}\boldsymbol{B}^{\mathrm{T}}(t)\boldsymbol{P}(t) + \boldsymbol{Q}\}\Delta \boldsymbol{X}(t) \tag{18}$$

The matrix $\boldsymbol{P}^{\mathrm{T}}(t)\boldsymbol{B}(t)(\boldsymbol{R}^{-1})^{\mathrm{T}}\boldsymbol{B}^{\mathrm{T}}(t)\boldsymbol{P}(t)$ is a positive definite matrix because R is a positive definite matrix and Q is a semi-positive definite matrix. Thus, $\boldsymbol{P}^{\mathrm{T}}(t)\boldsymbol{B}(t)(\boldsymbol{R}^{-1})^{\mathrm{T}}\boldsymbol{B}^{\mathrm{T}}(t)\boldsymbol{P}(t) + \boldsymbol{Q}$ is a positive definite matrix. Thus, we have $\dot{V} < 0$. By now, we draw the conclusion that the control system is stable.

5. Experiments and analysis

The firing practice system is mainly composed of several target robots, a client, and a remote controller. In this section, we put emphasis on the control of the mobile target robot which is the most important component of the firing practice system. The picture of the mobile target robot is shown in Fig. 4.

The mobile target robot can be divided into two parts: a mobile platform and a target control unit which can be easily replaced by other mission payloads. The shells of these two parts are made of bulletproof materials. The front surface of the mobile platform is designed to have a 45° slop and an anti-ricochet cover fixed to it, so as to prevent trainees from being hurt because of the ricochet. The laser transmitter is fixed behind the mobile target robot, and the laser spot, which only can be seen from the back of the target robot, is projected on the cut-beam flaps. Due to this design, the laser beam cannot be seen by the trainees, which avoids exerting influence on the shooting practice.

5.1. Experimental setup

A series of experiments, including indoor and outdoor experiments, were carried out to verify the feasibility of the method proposed in this paper.

https://doi.org/10.1017/S0263574720000545 Published online by Cambridge University Press

Table I. Experimental setup.

Laser parameters	
Transmitter power	100 mw
Transmitter size	D16 × 70 mm
Laser beam	635 nm
Product model	ZLM5AX635
Company	SHHO, China
Camera parameters	
Pixels	640 × 480
Optical parameters	F2.0 78°
Output	60 fps
Product model	ov7725 CMOS
Company	ZDYZ, China
Mobile platform	
Size of the cut-beam flap	220 × 75 mm
Size of the rectangular orifices	200 × 60 mm
Height of the camera lens	120 mm
Distance between two cut-beam flaps	450 mm

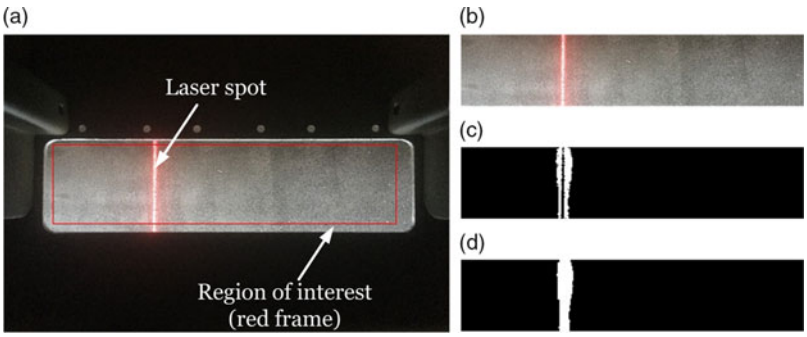


Fig. 5. Image processing by using the HSV feature extraction method. (a) Original image captured by camera; (b) ROI of the original image; (c) binary image; (d) image after morphological operation.

A laser transmitter was used to generate a laser beam. Two identical cameras, which were mounted inside the mobile platform and above two cut-beam flaps, were used to capture the images of the laser spots. The specific parameters of the laser transmitter, the cameras, and the key parameters of the mechanism are listed in Table I.

5.2. Vision-based Localization

The original image captured by the camera is shown in Fig. 5 (a). The laser spot is identified by using the HSV features extracting method, in order to prevent the ignorable influence of the ambient light in some shooting ranges. The ROI of the RGB image, as shown in Fig. 5 (b), is converted to an HSV image at first. Then, the binary image, as shown in Fig. 5 (c), is obtained by using a threshold of [0, 40] and [200, 255] respectively for the hue component and [40, 255] for the saturation component. A morphological operation is adopted to remove the narrow gap at the center of the laser spot, and hence an image with a clearly demarcated laser spot is obtained as shown in Fig. 5 (d). At last, the very center of the laser spot can be easily established by Eq. (10) proposed in subsection 3.2.

5.3. Tracking control

In the application, the mobile target robots must track along the laser beam with a certain speed, so as to act like a terrorist running towards the trainees. Thus, the tracking effects are critical for the mobile target robot. In order to estimate the feasibility of the proposed LQR control method, a conventional

https://doi.org/10.1017/S0263574720000545 Published online by Cambridge University Press

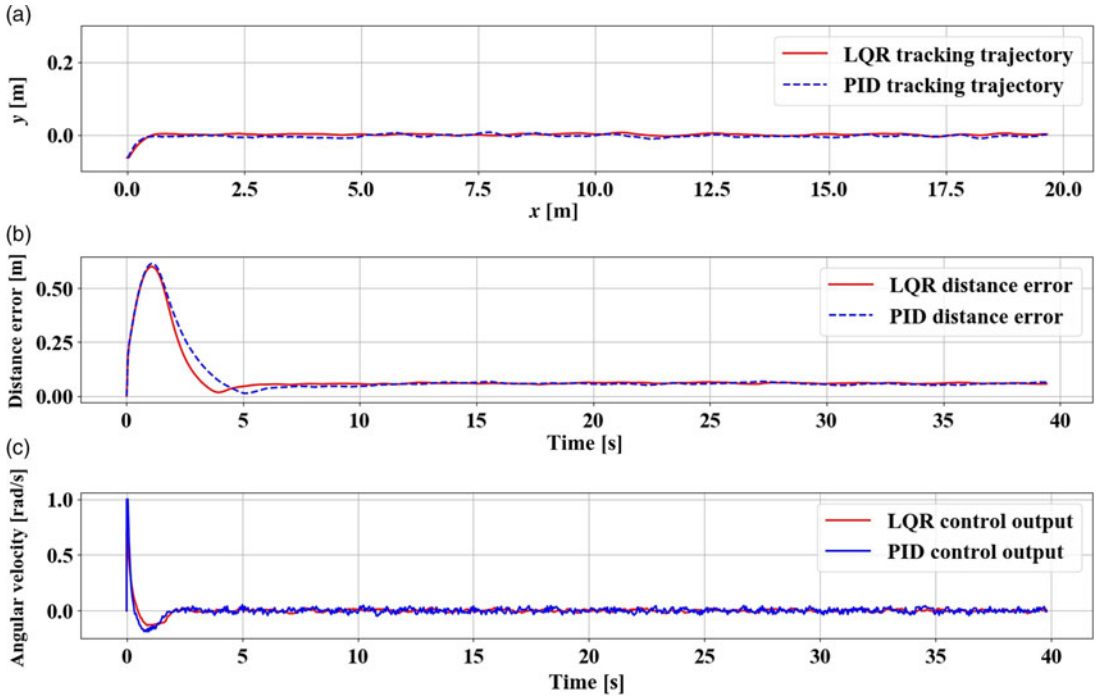


Fig. 6. Results of the tracking control. (a) Lateral error during tracking. (b) Distance error between the position of the robot and the referenced position. (c) Angular velocity output.

PD controller was adopted and performed in the experiments as well, the control law of which is as follows:

$$\begin{cases} e_{syn} = w \cdot e_{dis} + (1 - w) \cdot e_{ori} \\ \omega = K_p^{\omega} \cdot e_{syn} + K_d^{\omega} \cdot (e_{syn} - e_{syn}^{old}) \\ v = K_p^{v} \cdot e_{pos} + K_d^{v} \cdot (e_{pos} - e_{pos}^{old}) + v^{old} \end{cases} \tag{19}$$

where $w \in [0, 1]$. K_p and K_d are the proportional and differential coefficients of the PD controller, and e_{pos} is the distance error between the referenced position and the actual position of the target robot. The symbols which have an "old" superscript denote that the variable is the value computed from the last control cycle.

In the comparative experiments, we set the parameters of the PD controller as $w = 0.5$, $K_p^{\omega} = 3.7$, $K_d^{\omega} = 11.4$, $K_p^{v} = 45$, and $K_d^{v} = 70$ after parameter regulation. Meanwhile, we set the parameter matrices of the LQR controller as $\boldsymbol{Q}$ = diag(1,3,1) and $\boldsymbol{R}$ = diag(1,1), respectively. The referenced linear and angular velocities are set to 2 m/s and 0 rad/s, respectively.

The tracking results are shown in Fig. 6. The lateral error is shown in Fig. 6 (a), from which we can observe that the LQR control is more stable than the PD control. Slight oscillation occurs when using PD control due to the existence of the noise in localization. This will cause problems in higher speed tracking. Therefore, it is necessary to introduce a recovery control method in the PD tracking control, such as the DWA. However, the LQR is more stable and robust against the noise in localization. Figure 6 (b) illustrates the distance error between the referenced position and the actual position of the mobile target robot. It shows that the position of the robot converges to the referenced position faster than PD control, which means the former achieves better results in linear velocity control. The reason for that is from Eq. (19), we can see that the linear velocity control and the angular velocity control are isolated, which can cause discordance between these two controls. Figure 6 (c) shows the angular velocity control outputs between these two control methods. It is obvious that the angular velocity control output of the PD control changes with greater amplitude, compared with the LQR control, owing to that the latter aims to reduce both the control energy and tracking error in the process of constructing the Riccati equation.

https://doi.org/10.1017/S0263574720000545 Published online by Cambridge University Press

Table II. Performance comparison.

Key indicators	**PD**	**LQR**
Converge time	5.1 s	4.2 s
Max lateral error (stable)	0.035 m	0.022 m
RMS lateral error (stable)	0.027 m	0.010 m
Max distance error	0.692 m	0.673 m
RMS distance error	0.320 m	0.276 m

RMS: Root Mean Square

The control performance comparison between the conventional PD control and the LQR control after 10-times tracking experiments is shown in Table II. The LQR control has better performance, in several key aspects including the time of converge, the lateral error, and the distance error, than that of the PD control in tracking the laser beam.

Note that the light density reduces dramatically when the distance between the laser transmitter and the cut-beam flaps is more than 20 m, which is determined by the power of the laser transmitter. The tracking control will be influenced or even failed when the light density of the laser spot is lower enough detected by cameras. For this reason, a more powerful laser transmitter enables a longer tracking in the application.

6. Conclusions

This paper proposed a complete solution for the laser beam tracking system that is used for the mobile target robot in shooting ranges. The mechanical design was illustrated, and the principle of which was explained in detail. The structure of control system was introduced and each component in it was explained. The laser spots projected on the cut-beam flaps were recognized by the HSV color space feature extraction method. Once the laser spots are located, the pose of the mobile target robot that is related to the laser beam can be established. Then, the LQR control was employed to achieve the stable tracking control along the laser beam. Finally, the mobile target was illustrated. The experiments were carried out, and the comparison, based on the tracking results, was analyzed between the conventional PD control and the LQR control. It verifies the feasibility of the proposed LQR control method for the laser beam tracking.

As for future studies, a more suitable laser transmitter, such as the infrared laser transmitter or the laser transmitter with more power, will be tested, in order to further reduce the influence to shooters or trainees and expand the tracking distance of the mobile target robot. Moreover, the paired optical filters should be designed to enhance the stability of image processing-based localization in various kinds of working environments.

References

1. National research council of the national academies, *Technology Development for Army Unmanned Ground Vehicles* (National Defense Industry Press, Beijing, 2009) pp.1–30.
2. L. Taponecco, A. A. D'Amico and U. Mengali, "Joint TOA and AOA estimation for UWB localization applications," *IEEE Trans. Wireless Commun*. **10**(7), 2207–2217 (2011).
3. G. Cicirelli, A. Milella and D. D. Paola, "RFID tag localization by using adaptive neuro-fuzzy inference for mobile robot applications," *Ind. Robot Int. J.* **39**(4), 340–348 (2012).
4. L. Zhang, R. Zapata and P. Lepinay, "Self-adaptive Monte Carlo localization for mobile robots using range finders," *Robotica*, Cambridge University Press. **30**, 229–244 (2012).
5. J. Park, W. S. Hwang, G. Jwon and K. Kim, "A novel line of sight control system for a robot vision tracking system, using vision feedback and motion-disturbance feedforward compensation," *Robotica* **31**, 99–112 (2012).
6. Y. J. Lyu, A. L. Xu, C. C. Chang and M. Y. Cao, "Application analysis of the linear CCD in the path recognition system," *Proceedings of the 2007 IEEE International Conference on Integration Technology*, Shen Zhen, Guangdong, China (Mar, 20–24, 2007) pp. 151–154.
7. H. S. Kim, W. Seo and K. Baek, "Indoor positioning system using magnetic field map navigation and an encoder system," *Sensors* **17**(3), 651–667 (2017).
8. S. Thrun, M. Mentemerlo and H. Dahlkamp, "Stanley: The robot that won the DARPA challenge," *J. Field Robot.* **23**(9), 661–692 (2006).
9. X. P. Meng, L. Kou and Q. Yuan, "Motion control of robot based on a new integral separated PID," *Int. J. Wireless Mob. Comput.* **11**(3), 207–213 (2016).

https://doi.org/10.1017/S0263574720000545 Published online by Cambridge University Press

10. A. Alouache and Q. H. Wu, "Fuzzy logic PD controller for trajectory tracking of an autonomous differential drive mobile robot," *Ind. Robot Int. J.* 45(1), 23–33 (2018).
11. B. Sebastian and B. T. Pinhas, "Active disturbance rejection control for handling slip in tracked vehicle locomotion," *J. Mech. Robot.* **11**(2), 389–399 (2019).
12. L. Pacheco and N. Luo, "Testing PID and MPC performance for mobile robot local path-following," *Int. J. Adv. Robot. Syst.* **12**(11), 155–171 (2015).
13. Z. Zhang, L. Wang and L. Li, "Design and implementation of two-wheeled mobile robot by variable structure sliding mode control," *Proceedings of the 35th Chinese Control Conference*, Chengdu, Sichuan, China (Jul, 29–29, 2016) pp. 5869–5873.
14. Z. P. Jiang and H. Nijmeijer, "Tracking control of mobile robots: A case study in backstepping," *Automatica* **33**(7), 1393–1399 (1997).
15. H. J. Zhang, J. W. Gong and Y. Jiang, "An iterative linear quadratic regulator based trajectory tracking controller for wheeled mobile robot," *J. Zhejiang Univ.* **13**(8), 593–600 (2012).
16. D. Fox, W. Burgard and S. Thrun, "The dynamic window approach to collision avoidance," *IEEE Robot. Autom. Mag.* **4**(1), 23–33 (1997).
17. J. Velagic, N. Osmic and B. Lacevic, "Neural network controller for mobile robot motion control," *Word Acad. Sci. Eng. Technol. Int. J. Electric. Comput. Eng.* **2**(11), 134–145 (2008).
18. N. T. Luy, N. T. Thanh and H. M. Tri, "Reinforcement learning-based intelligent tracking control for wheeled mobile robot," *Trans. Institute Meas. Control* **36**(7), 868–877 (2014).
19. R. C. Gonzalez and R. E. Woods, *Digital Image Processing* (3rd edition) (Publishing House of Electronics Industry, Beijing, 2017) pp. 249–284.
20. X. Y. Zhang, X. Q. Wang and F. Z. Bai, "A gray centroid method based light band center recognition algorithm," *Laser Infrared* **46**(5), 622–626 (2016).

https://doi.org/10.1017/S0263574720000545 Published online by Cambridge University Press